Monthly Notices
of the
ROYAL ASTRONOMICAL SOCIETY

MNRAS **458,** 4238–4249 (2016)
Advance Access publication 2016 March 14

doi:10.1093/mnras/stw585

Tracking the energetics of the non-thermal disc–corona–jet in the very high state GX 339 − 4

A. Kubota[1⋆†] and C. Done[2⋆]

[1]*Department of Electronic Information Systems, Shibaura Institute of Technology, 307 Fukasaku, Minuma-ku, Saitama-shi, Saitam 337-8570, Japan*
[2]*Department of Physics, University of Durham, South Road, Durham DH1 3LE, UK*

Accepted 2016 March 9. Received 2016 March 9; in original form 2015 August 17

ABSTRACT

The dramatic hard–soft spectral transition in black hole binaries is important as it is associated with the collapse of the jet and with the strongest low-frequency quasi-periodic oscillations (QPOs). These transition spectra (intermediate and very high state: VHS) are complex, with soft but distinctly non-thermal Comptonization which merges smoothly into the disc emission. Here we develop a physical model for the accretion flow which can accommodate all these features, with an outer standard disc, which can make a transition to an energetically coupled disc–corona region, and make a further transition to a hot inner flow which can be radiatively inefficient if required. The code explicitly uses fully relativistic emissivity (Novikov–Thorne), and all Comptonization is calculated with a hybrid (thermal and non-thermal) electron distribution. We fit this to a VHS spectrum from GX 339 − 4. We show that the complex continuum curvature produced by a hybrid electron distribution is enough to remove the strong constraint on black hole spin derived from reflection using simpler Comptonization models. More fundamentally, we show that the VHS cannot be fit with the same Novikov–Thorne emissivity which can fit the disc-dominated spectrum but instead requires that the inner flow is somewhat radiatively inefficient. This is consistent with an accretion powered jet, but simultaneous radio data show that the jet has already collapsed at the time of our data. Instead, it could point to truncation of the inner flow at radii larger than the innermost stable circular orbit, as predicted by the Lense–Thirring QPO models.

Key words: accretion, accretion discs – black hole physics – radiation mechanisms: general – X-rays: individual: GX 339–4.

1 INTRODUCTION

The two best known black hole binary states are the low/hard and high/soft states. The low/hard state is dominated by hard (photon index $\Gamma < 2$) Comptonized emission from a hot, optically thin flow whereas the high/soft state is instead dominated by soft, blackbody emission from a cool, optically thick disc. The transition between these two states is generally interpreted in terms of the truncated disc model, where in the low/hard state the inner thin, cool, radiatively efficient disc evaporates into a geometrically thick, hot, advection-dominated flow (e.g. Esin, McClintock & Narayan 1997). Spectra around the transition are rather rare since the transitions are fast, but these (hard and soft) intermediate states (HIMS/SIMS) show both a strong disc and strong but soft ($\Gamma \sim 2.5$–3) Comptonized tail. There is also a distinct branch, the very high state (VHS), on the hardness-intensity diagram at the highest luminosity where the spectral shape is similarly a composite of a strong disc and strong, steep Comptonized spectrum (Remillard & McClintock 2006; Done, Gierliński & Kubota 2007).

These transition spectra are of especial importance as they are associated with dramatic changes in the radio emission from the jet. The steady compact jet seen in the low/hard state (Gallo, Fender & Pooley 2003; or Corbel et al. 2013b for an up to date version) collapses as the source makes a transition to the disc-dominated states. This collapse takes place via discrete plasma ejection events which can impact into the previous jet material, producing optically thin synchrotron emission from internal shocks (Fender, Belloni & Gallo 2004). Extrapolating back from the observed proper motion of the shocked radio plasma indicates that the initial ejection takes place around the time where the fast X-ray variability properties change dramatically (e.g. Miller-Jones et al. 2012). The ubiquitous broad-band noise seen in the X-ray variability in the low/hard state suddenly collapses, correlated with a more subtle change in the low-frequency quasi-periodic oscillation (QPO) from type C to B, and

† E-mail: aya@shibaura-it.ac.jp (AK); chris.done@durham.ac.uk (CD)
⋆ Affiliated to Durham University.

an even more subtle spectral softening (from HIMS to SIMS). It is very tempting to associate this very obvious change in timing signature with the ejection event (jet line; Fender et al. 2004), but this is probably not a causal connection as some objects with good monitoring campaigns show that the radio collapses before the change in timing (GX 339 − 4: Fender et al. 2009; MAXI J1659 − 152: van der Horst et al. 2013).

None the less, the steady compact jet is normally seen together with the type C QPO. The current best model for this QPO involves Lense–Thirring (vertical) precession of the entire hot inner flow region within the truncated disc (Ingram, Done & Fragile 2009), so this associates the steady jet with a geometrically thick, hot inner flow. However, testing whether this truncated disc/hot inner flow geometry really does apply in the HIMS/VHS spectra is not easy.

The inner edge of the thin disc can be tracked in the disc-dominated states, and is consistent with extending down to a fixed inner radius despite large changes in mass accretion rate (Kubota, Makishima & Ebisawa 2001; Kubota & Makishima 2004; Done et al. 2007). However, the HIMS/VHS are characterized by strong soft Comptonization of the disc emission, which can distort the observed disc emission in two ways. First, strong Comptonization implies that not all of the accretion energy is dissipated in the disc. In a disc–corona geometry, this means that the underlying disc is cooler and less luminous than expected (Poutanen & Svensson 1996). Secondly, the Comptonization process itself removes photons from the disc spectrum to scatter them into the Compton spectrum. Thus, there is coupling of both energy and photon number between the disc and Comptonization region. In the studies of Kubota & Done (2004), Done & Kubota (2006) and Tamura et al. (2012; hereafter T12), we assumed that this coupling was between a disc and thermal Compton component. However, the strong Compton tail in the VHS/HIMS is often seen to have a composite shape, requiring a non-thermal electron distribution as well as thermal electrons (Zdziarski et al. 2001; Gierliński & Done 2003; Hjalmarsdotter, Axelsson & Done 2016). In our previous work, we assumed that this non-thermal emission had negligible impact on the energy and photon coupling between the disc and corona. This is not necessarily true.

In this paper, we build a new model 'DISKEQ' to explore the geometry and energetics of these complex HIMS/VHS. We use the Novikov–Thorne thin disc emissivity to specify the local energy release. At large radii we assume that this emission is dissipated as a (colour temperature corrected) blackbody as in a standard disc. We allow this to make a transition in the inner region to an energetically coupled disc–corona, where the coronal electrons can have a hybrid (thermal and non-thermal) electron distribution, modelled using the EQPAIR code (Coppi 1992). We then allow the disc–corona to make a further transition to a hot inner flow, where again the electrons can have a hybrid electron distribution.

We use this to fit the VHS/HIMS spectrum of a black hole binary GX 339 − 4 observed with *Suzaku*, and compare this with a disc-dominated spectrum seen from the same object three days later with *XMM–Newton* and *RXTE* in order to get the best possible constraints on any change in geometry and energetics between these two states.

In Section 2, we describe observations of the VHS with *Suzaku* and the high/soft state with *XMM* and *RXTE*. Details of the new model are given in Section 3. The high/soft state spectrum is fit in Section 4. This is disc dominated, so it constrains black hole spin. This is rather low for our assumed system parameters, in conflict with the very high black hole spin derived from a recent re-evaluation of the iron line profile in multiple data sets, including the VHS *Suzaku* data studied here (Ludlam, Miller & Cackett 2015). We fit the VHS spectra first with simple models in Section 5 and show that the high spin/high reflected fraction derived by Ludlam et al. (2015) is degenerate with the continuum complexity which comes from allowing a hybrid (rather than purely power law) electron distribution. We then fit the VHS spectra with our new disc model, to show that it requires an inner flow which is underluminous compared to the mass accretion rate inferred through the outer disc. While this might signal that a substantial fraction of the accretion luminosity is used to power the jet, the absence of strong radio emission during this observation makes this unlikely. We conclude that either the flow has not yet reached steady state from the rapid rise to outburst and/or that the Novikov–Thorne accretion emissivity derived for a thin disc is not appropriate for the more complex accretion flow geometry considered here.

2 OBSERVATION AND DATA REDUCTION

As described in T12, the 2006/2007 outburst of GX 339 − 4 was its brightest outburst since the launch of *RXTE* in 1995. The light curves and hardness ratio of this outburst (fig. 1 of T12) showed that the state transition occurred around MJD≃54140–54150, and that the *Suzaku* observation was performed just before the peak of the *RXTE* count rate (MJD 54143.2–54146.2; 2007 February 12 05:33:31 to 15 04:48:26). Both the QPO (type C, increasing from 4.3 to 5.5 Hz) and spectral properties (Γ increasing from 2.6–2.7) characterize the source as being in the VHS during the *Suzaku* observation (T12).

Data reduction is described in T12, but we redo this by AEPIPELINE (VERSION 1.1.0) implemented in HEASOFT 6.16 using the same selection but with the latest calibration files released on 2014 June 24. As before, we mitigate pileup in the XIS by using only XIS0 data, and extract events from a circular annulus from 7 to 3 arcmin, to exclude the core (Yamada et al. 2009). Further excluding events with telemetry saturation gave an exposure time of 2.83 ks out of the total 12.4 ks observation. We use the XIS0 data from 0.7 to 1.5 keV and 2.3 to 10 keV, including 1 per cent systematic error on each energy bin.

We similarly reprocessed the hard X-ray detector (HXD; Kokubun et al. 2007) data from both PIN and GSO data with AEPIPELINE with their standard criteria. Following T12, both the non-X-ray background (NXB) and the cosmic X-ray background were subtracted from the PIN spectrum, and only NXB was subtracted from the GSO spectrum. For the spectral analyses, we used 12–70 keV PIN data with the response matrix of AE_HXD_PINXINOME3_20080129.RSP, and used 50–200 keV GSO data with the response matrixes of AE_HXD_GSOXINOM_20100524.RSP and AE_HXD_GSOXINOM_CRAB_20100526.ARF (Yamada et al. 2011). Systematic errors of 1 per cent were added to each energy bin for the PIN spectrum. We also added 0.5 per cent to the GSO background spectrum to consider the effect of a systematic uncertainty of up to 3 per cent in the GSO background. The cross-normalization of PIN and GSO to XIS0 are fixed at 1.16,[1] since the observation was performed at the XIS nominal position.

We use the high/soft state data from *XMM* and *RXTE* taken at the peak of the *RXTE*/ASM count rate (MJD 54150.01–54150.20; 2007 February 19 00:20:54 to 04:43:28). The *XMM–Newton* data are in burst mode, with net exposure of 448 s, while the contemporaneous *RXTE* data have net exposure of 3.23 ks (see Kolehmainen, Done & Díaz Trigo 2011). We use the energy range 0.6–2.0 keV and

[1] ftp://legacy.gsfc.nasa.gov/suzaku/doc/xrt/suzakumemo-2008-06.pdf

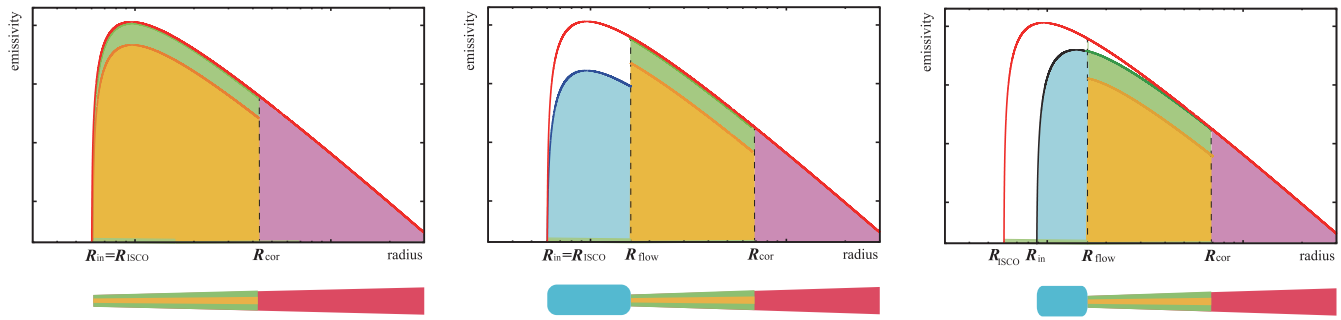

Figure 1. Schematic picture of accretion disc structure and local emissivity of disc without inner flow (left), disc with inefficient inner flow (middle), and disc with stress-free truncated inner flow (right). Novikov–Thorne model, blackbody emission from the outer disc, blackbody emission from the middle part, EQPAIR from the middle part, and the Comptonized emission from the inner plasma are shown with solid red lines, magenta, orange, green, and blue, respectively.

2.4–10 keV for the *XMM*/PN, 7–30 keV for the *RXTE*/PCA, and 30–150 keV for the *RXTE*/HEXTE. We use systematic errors of 1 per cent to the each energy bin for the *XMM*/PN spectrum. This is lower than the 2 per cent used by Kolehmainen et al. (2011) as we do not include the *RXTE* data in the energy range of 3–7 keV where the cross-calibration errors are large (Kolehmainen et al. 2011).

3 DISKEQ MODEL

The energetically coupled disc and corona model, DKBBFTH (Done & Kubota 2006), used to fit these data in T12 is based on the DISKBB (Mitsuda et al. 1984) emissivity, i.e. assumes that the local energy release is proportional to R^{-3} in the disc over all radii from $R_{\rm out}$ down to $R_{\rm in}$. This gives a temperature distribution $T(r) = T(R_{\rm in})(R/R_{\rm in})^{-3/4}$ if it thermalizes to a blackbody, so it is parametrized by an inner disc temperature, $T(R_{\rm in})$, and radius $R_{\rm in}$. We upgrade this to use the fully general relativistic Novikov–Thorne emissivity (Novikov & Thorne 1973), which includes the full stress-free inner boundary condition. The free parameters are then the three physical parameters of mass, mass accretion rate, and black hole spin.

As in DKBBFTH, the model assumes that this energy is dissipated as an optically thick blackbody from $R_{\rm out}$ to $R_{\rm cor}$. However, the optically thick disc emission is now explicitly corrected for electron scattering in the disc via a self-consistently calculated colour temperature correction (Done et al. 2012), rather than having this as an additional free parameter. We calculate the colour temperature corrected blackbody flux on a radial grid with at least 20 points per decade.

We then use the EQPAIR[2] code (e.g.Coppi 1992) to describe the Comptonization, so that the electron distribution can be a mix of thermal and non-thermal (hybrid). The spectral shape of EQPAIR is parametrized using the ratio of power injected into the electrons (hard power, $L_{\rm h}$) to the luminosity of seed photons intercepted by the source (seed photon luminosity, $L_{\rm s}$). Both these are parametrized as a compactness, i.e. a dimensionless luminosity to size ratio i.e. $\ell = L/R \times \sigma_{\rm T}/(m_e c^3)$, and the ratio $L_{\rm h}/L_{\rm s} = \ell_{\rm h}/\ell_{\rm s}$. A further parameter sets the fraction of non-thermal acceleration compared to the total (non-thermal plus thermal) electron power $\ell_{\rm nth}/\ell_{\rm h}$. Any non-thermal electrons are assumed to be injected with a power-law spectrum, $Q(\gamma) \propto \gamma^{-\Gamma_{\rm inj}}$, between $\gamma_{\rm min}$ and $\gamma_{\rm max}$ while the thermal ones have a Maxwellian distribution. Both thermal and non-thermal electrons cool via Compton and Coulomb collisions to form a self-consistent hybrid electron distribution, $N(\gamma)$. Even completely non-thermal acceleration gives a steady-state distribution which is thermal at low energies due to the effect of Coulomb collisions. We fix the minimum and maximum electron Lorentz factors $\gamma_{\rm min}$ and $\gamma_{\rm max}$ at 1.3 and 1000, respectively, leaving only $\Gamma_{\rm inj}$ as the free parameter of the non-thermal electron injection. The code includes the effects of photon–photon pair production, so the self-consistent electron optical depth $\int N(\gamma)\sigma_{\rm T} R {\rm d}\gamma = \tau = \tau_{\rm p} + \tau_{\rm e^{\pm}}$.

We consider several geometries for the electrons in the VHS, as shown schematically in Fig. 1. First (Fig. 1a), we assume the Comptonizing corona overlies the inner portion of an untruncated inner disc as in the DKBBFTH model but with the more flexible EQPAIR model to describe the Comptonized emission, allowing the electrons to be non-thermal as well as thermal. We assume that all the electron parameters remain constant with radius in the coupled disc–corona region, and that the accretion power dissipated in radii between $R_{\rm cor}$ to $R_{\rm ISCO}$ is split between the disc and corona, with a fraction f powering the corona, and the remaining $(1-f)$ powering the underlying disc (Haardt & Maraschi 1993; Svensson & Zdziarski 1994). Hence the underlying disc emission is both less luminous and cooler than a pure disc without a corona. However, there is also reprocessing of the hard X-rays in the disc, which adds to the seed photons, so the ratio of coronal power to seed photon luminosity, $\ell_{\rm h}/\ell_{\rm s}$, which is the major determinant of the shape of the spectrum is not simply $f/(1-f)$. Instead, we use $l_{\rm h}/l_{\rm s}$ derived from the shape of the spectrum to define a new parameter $g = \ell_{\rm h}/(\ell_{\rm s} + \ell_{\rm h})$ which includes the contribution of reprocessed/reflected flux. The relation of g to f is described in Appendix B, but they are equal only if the albedo $a = 1$ in the coupled disc–corona region, so that all the flux is reflected rather than reprocessed.

We calculate Comptonization locally, splitting the coupled disc–corona region up into multiple regions, again using a radial grid with at least 20 points per decade. The soft compactness in each annulus of width ${\rm d}R$ is $\ell_{\rm s} = [(1-g)L_{\rm NT}(R)4\pi R {\rm d}R/R] \times (\sigma_{\rm T}/m_e c^3)$, while the intrinsic hard compactness is $\ell_{\rm h} = [gL_{\rm NT}(R)4\pi R {\rm d}R/R] \times (\sigma_{\rm T}/m_e c^3)$.

The EQPAIR code returns both transmitted (unscattered) seed photons and Comptonized photons together, but the transmitted seed photons can be separately calculated with a second call to EQPAIR using the sign of the seed photon compactness as a switch[2]. We use this to separate out the Comptonized and unscattered seed photons, at each radius, and then add together the Comptonized seed photons from all anuuli to form a single Comptonized spectrum for plotting purposes, and for convolution with the RFXCONV and KDBLUR models

[2] http://www.astro.yale.edu/coppi/eqpair/eqpap4.ps

to produce the self-consistent ionized reflected emission from this region. Similarly we add together all the unscattered seed photons from all radii in the coupled disc–corona region, again so that we can show these as a single component for plotting.

We also consider the case where the innermost radius of the coupled disc–corona is truncated before the innermost stable circular orbit (ISCO), where the remaining power is dissipated in a hot inner flow. This geometry allows a smooth transition between the truncated disc models used for the low/hard state and the VHS geometry. This inner flow region is also required by the Lense–Thirring precession models for the low-frequency QPO as a vertical oscillation is suppressed if there is a disc in the mid-plane (Ingram et al. 2009). We again use EQPAIR to model this Comptonized emission so that this can also be non-thermal/hybrid, and set $\ell_{\rm h}$ from the remaining accretion power between where the disc truncates, $R_{\rm flow}$, and $R_{\rm ISCO}$, i.e. we assume $L_{\rm h} = f_{\rm rad} \int_{R_{\rm flow}}^{R_{\rm ISCO}} L_{\rm NT}(R) 4\pi R {\rm d}R$ where $f_{\rm rad} \leq 1$ is a factor to allow the flow to be radiatively inefficient as might be the case if it powers a strong jet. This sets $\ell_{\rm h} = L_{\rm h}/R_{\rm flow} \times \sigma_{\rm T}/(m_e c^3)$.

In this inner region, we only calculate a single EQPAIR model as we assume a single seed photon temperature which is set by that of the innermost edge of the disc i.e. that they are a blackbody with temperature equal to that of the disc in the coupled disc–corona region (or the standard outer disc if $R_{\rm cor} = R_{\rm flow}$ when the coupled coronal region does not exist). These seed photons for the inner region are produced in at different radius, so their energy adds to that released in the inner region. It is not removed from the region where the seed photons are generated as these photons are intercepted by the corona along a different line of sight than is observed. Hence only the Comptonized photons are seen, as any seed photons which are transmitted rather than scattered are not in the observers direction. The fraction of seed photons which intercept the flow depends on the detailed structure of the corona (scaleheight, and radial electron emissivity). Since these are unknown, we set $\ell_{\rm h}$ as above, then have $\ell_{\rm h}/\ell_{\rm s}$ as a free parameter and then determine after the fit whether the required $L_{\rm s}$ is physically reasonable e.g. a spherical source within a truncated disc can intercept at most 1/3 of the photons from the disc (Gardner & Done 2013). Again we separate out the Comptonized photons (using the sign of $R_{\rm flow}$ as a switch) so as to be able to compute the self-consistent reflected emission.

4 CALIBRATING THE EMISSIVITY FROM THE HIGH/SOFT STATE

To investigate geometry of the disc and corona in the VHS, the standard value of the spin (or a value of the ISCO) is required. In this section, we present the analysis of the high/soft state spectrum obtained with *XMM* and *RXTE*.

4.1 Standard modelling

In order to characterize the spin parameter based on the standard modelling of emission from the optically thick and geometrically thin disc, we first model the disc emission in the high/soft state with a Novikov–Thorne emissivity disc KERRBB (Li et al. 2005), convolved with SIMPL (Steiner et al. 2009) to model the weak Compton tail. Following T12, the distance, mass and inclination are assumed to be $D = 8$ kpc, $M = 7\,{\rm M}_{\odot}$ and $i = 50^{\circ}$, respectively. The Compton tail illuminates the disc and forms an ionized reflection component, modelled using the convolution model RFXCONV, which calculates the reflected spectrum and iron line from an X-ray illuminated slab including Compton scattering (Kolehmainen, Done & Díaz Trigo 2011). The reflected spectrum was smeared by general relativistic effects using KDBLUR(Laor 1991). The parameters of the smeared reflection are fixed at iron abundance $A_{\rm Fe} = 1$, inclination $i = 50^{\circ}$, $R_{\rm in} = 6\,R_{\rm g}$, $R_{\rm out} = 400\,R_{\rm g}$, and power-law illumination emissivity index of $\beta = 3$.

Here and hereafter, all the model components are absorbed by a common hydrogen column models with the Tuebingen–Boulder ISM absorption model (TBABS) under the abundance by Wilms, Allen & McCray (2000). The model is described as TBABS(SIMPL*KERRBB+KDBLUR*RFXCONV*SIMPL$_{\rm comp}$* KERRBB) in XSPEC. To use the convolution models, SIMPL, RFXCONV, and KDBLUR, we extended the energy band from 0.1 to 1000 keV. The KERRBB model with limb-darkening and without returning radiation reproduced the spectrum well with $\chi^2/{\rm dof} = 205.2/213$, and gave an absorbed 0.7–100 keV flux of 2.36×10^{-8} erg s^{-1} cm^{-2}. All the parameters are given in column (1) in Table 1, and the best-fitting spin parameter of $a^* = 0.11^{+0.02}_{-0.01}$ indicates $R_{\rm ISCO}$ of $5.6\,R_{\rm g}$. The residuals between the data and model are shown in Fig. 2(b), and unabsorbed model spectrum is shown in the left-hand panel of Fig. 3.

We replaced the KERRBB model with the simpler DISKBB. This did not give an acceptable fit, with $\chi^2/{\rm dof} = 288.4/213$ (see column 2 in Table 1), as the relativistic effects included in KERRBB give a significantly broader disc spectrum. However, the derived apparent inner radius of $r_{\rm in} = 54$ km is consistent with the ISCO of non-spinning black hole, $6\,R_{\rm g}$, of $7\,{\rm M}_{\odot}$. Here the true inner radius is estimated by $\kappa^2 \xi r_{\rm in}$ as $\sim$63 km with the colour hardening factor $\kappa = 1.7$ (Shimura & Takahara 1995) and the correction factor for inner boundary condition of $\xi = 0.41$ (Kubota et al. 1998). We caution that the absolute values of spin depend strongly on the assumed black hole mass, distance, and inclination (see e.g. Kolehmainen & Done 2010) but here we are interested only in comparative rather than absolute radii as the focus of this paper is whether inner radius of the thin disc component is truncated in the VHS with respect to the disc-dominated high/soft state.

4.2 DISKEQ without the corona

We replaced the KERRBB model in the fits above with our new disc–corona model DISKEQ. First, we use this without any coronal emission, i.e. using this a purely Novikov–Thorne optically thick disc like KERRBB, but without the relativistic corrections. DISKEQ, similarly to OPTXAGNF Done et al. (2012), is for an angle averaged disc, so we incorporate inclination by fixing the normalization to $\cos i/0.5 = 1.287$ rather than unity. We use this together with the SIMPL and RFXCONV models to describe the weak Compton tail and its reflection. We get a poor fit, with $\chi^2/{\rm dof} = 297.0/213$, similar to that derived from the DISKBB fit above, but again the spin is low, at $a^* = 0.12$. This shows first that the self-consistent colour temperature correction used in DISKEQ is close to 1.7 as assumed for the KERRBB fits, and secondly that it is indeed relativistic smearing as opposed to the detailed shape of the Novikov–Thorne emissivity which gives the better fit of KERRBB compared to DISKBB.

We can approximate the effect of relativistic smearing into the disc model using KERRCONV (Brenneman & Reynolds 2006) by tying its spin parameter to that of DISKEQ, fixing the emissivity index to -3, inner convolution radius equal to $R_{\rm ISCO}$ and the outer at $2\,R_{\rm ISCO}$ (Done et al. 2013). This improves the fit significantly with $\chi^2/{\rm dof} = 208.7/213$ (Table 1), but the best-fitting value of the spin is similar, at $a^* = 0.06$. Thus relativistic corrections can affect the quality of the fit, but do not significantly change the best-fitting parameters. The residuals between the data and this model are shown in Fig. 2(c), the unabsorbed model spectrum is shown in middle

Table 1. The best-fitting parameters for the high soft state spectrum fitted with SIMPL*KERRBB (column 1), SIMPL*DISKBB (column 2), relativistically smeared SIMPL*DISKEQ without coupled corona (column 3), and DISKEQ with coupled corona (column 4).

Component	Parameter	(1) SIMPL*KERRBB[a]	(2) SIMPL*DISKBB	(3) SIMPL*DISKEQ[d]	(4) DISKEQ(DISC–CORONA)
TBABS	$N_{\rm H}(10^{21}\,{\rm cm}^{-2})$	$6.86^{+0.04}_{-0.03}$	6.57 ± 0.05	6.77 ± 0.05	$6.72^{+0.05}_{-0.02}$
SIMPL	Γ	$2.64^{+0.05}_{-0.09}$	$2.61^{+0.10}_{-0.09}$	$2.55^{+0.10}_{-0.09}$	–
	$f(10^{-2})$	$3.2^{+0.2}_{-0.1}$	3.3 ± 0.2	3.0 ± 0.2	–
RFXCONV[a]	$\Omega/2\pi$	$1.3^{+0.5}_{-0.4}$	$1.1^{+0.5}_{-0.3}$	$1.0^{+0.4}_{-0.3}$	$1.7^{+0.5}_{-0.2}$
	$\log \xi$	<1.72	$2.61^{+0.11}_{-0.14}$	$2.35^{+0.03}_{-0.04}$	$2.0^{+0.2}_{-0.4}$
DISKBB	$T_{\rm in}$ (keV)	–	$0.868^{+0.003}_{-0.002}$	–	–
	$r_{\rm in}$ (km)	–	54.2 ± 0.4	–	–
KERRBB[b]	$l_{\rm h}/l_{\rm s}$	–	–	–	$0.068^{+0.003}_{-0.004}$
or DISKEQ[c]	$\tau_{\rm cor}$	–	–	–	$0.13^{+0.03}_{-0.02}$
	$R_{\rm cor}(R_{\rm G})$	–	–	–	46^{+9}_{-8}
	$\dot{M}(10^{18}\,{\rm gs}^{-1})$	4.33 ± 0.04	–	$3.93^{+0.19}_{-0.18}$	$3.99^{+0.05}_{-0.02}$
	a^*	0.115 ± 0.010	–	$0.057^{+0.017}_{-0.015}$	$0.066^{+0.033}_{-0.035}$
χ^2/dof		205.2/213	288.4/213	208.7/213	211.3/212
Absorbed 0.7–100keV flux	$10^{-8}\,{\rm erg\,s^{-1}\,cm^{-2}}$	2.36	2.36	2.36	2.36
Unabsorbed 0.7–100keVflux	$10^{-8}\,{\rm erg\,s^{-1}\,cm^{-2}}$	3.27	3.21	3.26	3.24
Unabsorbed 0.1–200 flux	$10^{-8}\,{\rm erg\,s^{-1}\,cm^{-2}}$	4.11	3.93	4.01	3.99

Note. Energy is extended from 0.1 to 1000 keV. Distance and inclination are assumed to be $D = 8$ kpc and $i = 50^\circ$. [a]The parameters of the smeared reflection are fixed at iron abundance $A_{\rm Fe} = 1$, inclination $i = 50^\circ$, $R_{\rm in} = 6\,R_{\rm g}$, $R_{\rm out} = 400\,R_{\rm g}$, and power-law illumination emissivity index of $\beta = 3$. [b]While returning radiation is not included, limb-darkening is included. [c]The hot inner flow is not included. A normalization factor, $\ell_{\rm nth}/\ell_{\rm h}$, and $\Gamma_{\rm inj}$ are fixed at 1.287, 1, and 3.5, respectively. [d]DISKEQ spectrum is relativistically smeared by convolved with KERRCONV, in which all the parameters are fixed (i.e. $\beta_1 = \beta_2 = -3$, break radius as $6\,R_{\rm g}$, $r_{\rm in} = R_{\rm ISCO}$, and $r_{\rm out} = 2R_{\rm ISCO}$).

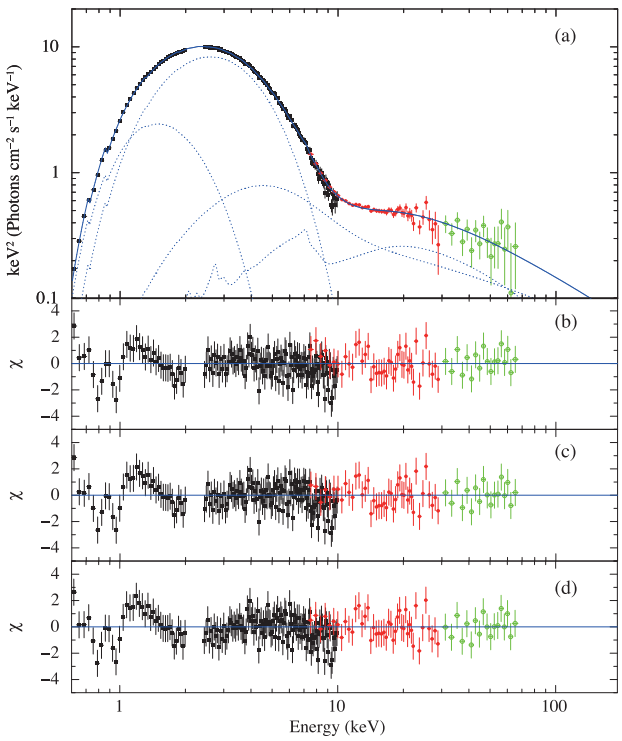

Figure 2. νF_ν spectrum and residuals between the data and the best-fitting models of GX339 − 4 in the high/soft state. Data points of pn, PCA, and HEXTE, are indicated with black filled square, red filled circle, and green open circle, respectively. The νF_ν spectrum is based in the best-fitting DISKEQ with hybrid corona (panel a). Residuals between data and the best fit KERRBB, relativistically smeared OPTXEQ without any corona, and OPTXEQ with corona are shown in panels (b), (c), and (d), respectively.

panel of Fig. 3 and all parameters are detailed in column (3) in Table 1.

4.3 DISKEQ with the corona

We now remove the SIMPL description of the Compton tail, and instead describe it self-consistently using the DISKEQ model, with $R_{\rm in} = R_{\rm ISCO}$ (see schematic geometry in the left-hand panel of Fig. 1). We reflect only the coronal emission via the switch in the code, using the convolution models RFXCONV and KDBLUR as before. The model is described as TBABS(DISKEQ + KDBLUR*RFXCONV*DISKEQ$_{\rm comp}$) in XSPEC.

To replicate the shape of SIMPL under the description of the DISKEQ, we fix $\ell_{\rm nth}/\ell_{\rm h} = 1$, i.e. assume completely non-thermal electron injection so as to get closest to the completely power-law Compton tail assumed in SIMPL. The SIMPL code also assumes that the entire disc emission at all radii is equally Compton scattered, so we set $R_{\rm cor} = 500\,R_{\rm g}$. We fix $\Gamma_{\rm inj} = 3.5$ (as required from a similar VHS spectrum from XTE J1550−564; Hjalmarsdotter et al. 2016) as this is not well constrained by our data. This gives χ^2/dof = 246.3/213 as the Comptonization in EQPAIR has a hybrid rather than pure power-law shape even for completely non-thermal injection. Coulomb collisions act to thermalize the electrons at low energy, giving rise to a low-temperature thermal Compton component which effectively smooths the transition between the Wien disc spectrum and power-law tail.

The fit improves still further to χ^2/dof = 211.3/212 by letting $R_{\rm cor}$ free. The unabsorbed model components are shown in the right-hand panel of Fig. 3. In addition to the low-temperature thermal Comptonization from the hybrid electron distribution (green), the best fit $R_{\rm cor} \sim 46\,R_{\rm g}$ means that the outer disc (magenta) is seen directly, while only the inner disc under the corona (orange) is slightly suppressed by the weak Comptonization, again resulting in

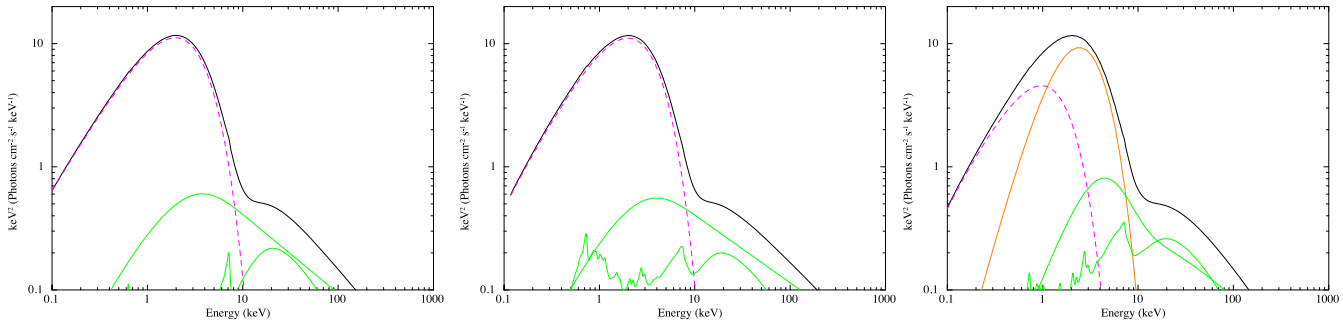

Figure 3. Unabsorbed spectral models for the high/soft state spectrum with *XMM* and *RXTE*, based on best-fitting models of KERRBB with SIMPL Comptonization (left), relativistically smeared DISKEQ with inner corona (middle), and DISKEQ with both coupled and inner corona (right). The model components shown separately are the disc (dashed magenta), inner coronal (or SIMPL) emission + its reflection (both solid green), and the coupled corona (orange, right-hand panel only).

a slight broadening of the observed disc emission. This fit is shown as the baseline νF_ν spectrum in Fig. 2(a), while its residuals are shown in Fig. 2(d). The best-fitting spin is again $a^* = 0.07$, and all parameters are given in column (4) in Table 1.

In conclusion, at these values of spin and inclination, the lack of relativistic effects on the disc emission is not as significant as the detailed geometry assumed for the disc and corona. Hence in all that follows we use DISKEQ without relativistic smearing. However, we also note that the derived reflection parameters are dependent on the details of how the continuum spectra are modelled e.g. the reflection solid angle is $\Omega/2\pi \sim 1$ with relativistic smearing of the disc continuum, significantly lower than the value ($\Omega/2\pi \sim 1.7$) derived without including this. This is because the relativistic smearing slightly broadens the disc emission, so the disc makes more of the continuum in the 5–8 keV range, requiring less reflection.

5 THE VERY HIGH STATE

5.1 Overview

We first illustrate the data using the SIMPL description of Comptonization, with TBABS(SIMPL*DISKBB + KDBLUR*RFXCONV * $\text{SIMPL}_{\text{comp}}$*DISKBB). This assumes that the seed photons are the entire disc, so all temperatures are equally scattered. This is an acceptable fit to the data, with parameters which require that the fit is reflection dominated, with $\Omega/2\pi = 4.8$, and that this reflection is highly smeared, with $R_{\text{in}} = 1.5$ and $\beta = 3.5$. This is in agreement with the study of Ludlam et al. (2015), where they use this model to argue that these data require a high spin black hole. The spectral decomposition using this model is shown in the left-hand panel of Fig. 4, and details of the fit are given in Table 2.

We then replace the SIMPL model with the EQPAIR description of Comptonization, where the spectrum is not a pure power law even for completely non-thermal acceleration. We assume that the seed photons are blackbody at the maximum disc temperature T_{in}. This gives a better fit to the data, and completely different reflection parameters. The amount of reflection is no longer enhanced, with $\Omega/2\pi = 0.8$, and there is little relativistic smearing. This illustrates how the spin parameter derived from reflection fits can be strongly affected by the choice of continuum. There is complex curvature in the data, which can be fit either by a large amount of highly smeared reflection on a power-law Comptonization continuum or by less reflection on the more physical EQPAIR continuum. We show this very different decomposition in the right-hand panel of Fig. 4 with

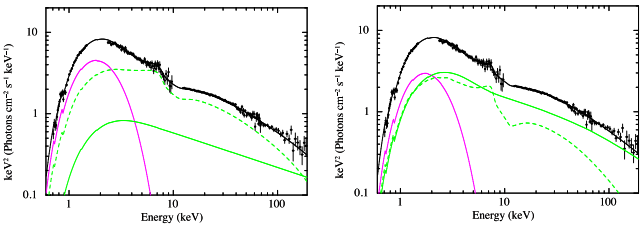

Figure 4. The *Suzaku* VHS spectrum fitted with SIMPL*DISKBB (left) and DISKBB+EQPAIR (right). The components are DISKBB (solid magenta), Comptonized DISKBB or Compton component of EQPAIR (solid green), and reflected emission (dashed green).

details of all parameters in Table 2. We caution that the reflection parameters are not always robust to a different continuum choice.

What is constant between both fits is the very low disc temperature, at ~0.5–0.6 keV. Fig. 5 shows comparison between the high/soft state spectrum and the VHS spectrum based on the best-fitting models of DISKEQ with hybrid corona and DISKBB+EQPAIR, respectively. A disc peaks in νf_ν at $2.35\,kT_{\text{in}}$ with i.e. at 1.2–1.4 keV. As shown in Table 2, the bolometric flux in the VHS is a factor of 1.1 larger than in the high/soft state, so this predicts that $\dot{M}$ also increases by a factor of 1.1. Thus a pure disc spectrum should peak at a very similar (slightly higher) energy than that of the high/soft state. Instead, as shown in Fig. 5, the VHS spectrum peaks at lower energy than the high/soft state. It is this decreasing energy at which the spectrum peaks which causes the models to struggle to fit these data.

Simply overlaying the inner disc with the Comptonizing corona does not help. Steep spectrum Comptonization retains the imprint of the seed photons, with a low-energy turnover at $7\,kT_{\text{bb}}$ for $\Gamma = 2.5$. On the contrary, the observed spectral peak is determined by the sum of this and the disc, with equal energy in both leading to a spectral peak at ~2 keV for a peak disc temperature of 0.53 keV (see the right-hand panel of Fig. 4). Thus the seed photons for the Comptonization must be no more than ~0.5 keV, when the expected inner disc temperature is ~1 keV. Covering the inner disc and using its energy to power the corona seems to be the obvious solution. However, the decrease in temperature produced by using a fraction g of the locally released gravitational energy to power the corona is $T = (1 - g)^{1/4}T_0$, so requires $g = 0.87$. This means that the majority of the power is released in the coronal region rather than in the underlying disc, though the steep spectrum shows very clearly that there is more energy in the seed photons than in the Comptonized emission.

Table 2. Overview of the *Suzaku* VHS spectrum.

Component	Parameter	SIMPL*DISKBB	DISKBB+EQPAIR
TBABS	$N_{\rm H}(10^{21}\ {\rm cm}^{-2})$	$6.72^{+0.19}_{-0.12}$	$6.91^{+0.15}_{-0.31}$
KDBLUR	β	3.5 ± 0.4	(3.0)
	$R_{\rm in}(R_g)$	$1.5^{+0.9}_{-0.3({\rm hardlimit})}$	$4.9^{+3.3}_{-1.4}$
RFXCONV	$\Omega/2\pi$	4.8 ± 1.1	$0.82^{+0.09}_{-0.12}$
	$\log\xi$	$3.71^{+0.07}_{-0.09}$	$4.0^{+0({\rm hardlimit})}_{-0.1}$
DISKBB	$T_{\rm in}$ (keV)	$0.580^{+0.013}_{-0.012}$	$0.526^{+0.014}_{-0.008}$
	$r_{\rm in}$ (km)	94 ± 5	92^{+4}_{-7}
SIMPL	Γ	$2.427^{+0.017}_{-0.021}$	–
	$f(10^{-2})$	$7.8^{+2.1}_{-1.8}$	–
EQPAIR[a]	$\ell_{\rm h}/\ell_{\rm s}$	–	0.28 ± 0.02
	τ	–	$0.67^{+0.08}_{-0.05}$
	Norm	–	$0.33^{+0.11}_{-0.03}$
χ^2/dof		228.9/198	214.5/198
Absorbed 0.7–100 keV flux	$10^{-8}\ {\rm ergs}^{-1}{\rm cm}^{-2}$	2.65	2.64
Unabsorbed 0.7–100 keV flux	$10^{-8}\ {\rm ergs}^{-1}{\rm cm}^{-2}$	3.58	3.61
Unabsorbed 0.1–200 keV flux	$10^{-8}\ {\rm ergs}^{-1}{\rm cm}^{-2}$	4.55	4.72

Note. Values in parenthesis are fixed. [a]Values of $\ell_{\rm nth}/\ell_{\rm h}$, $\gamma_{\rm min}$, $\gamma_{\rm max}$, and $\Gamma_{\rm inj}$ are fixed at 1, 1.3, 1000, and 3.5, respectively.

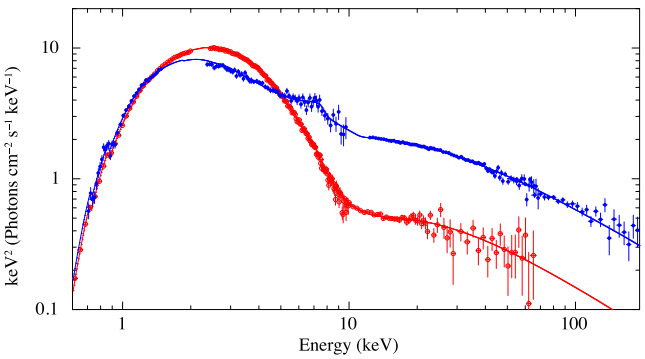

Figure 5. Comparison of νF_ν spectra of the high/soft state (red) and the VHS (blue). This is basically same as Fig. 7 in T12, but based on the best-fitting models of DISKEQ with coupled corona and DISKBB+EQPAIR, respectively.

A steep spectrum with $\Gamma \sim 2.5$ requires $\ell_{\rm h}/\ell_{\rm s} \sim 0.5$, i.e. $g = \ell_{\rm h}/(\ell_{\rm s} + \ell_{\rm h}) \sim 0.3$ (T12) whereas $g = 0.87$ implies $\ell_{\rm h}/\ell_{\rm s} \sim 7$. The soft Comptonized spectral shape is then at odds with the strong energy dissipation in the corona required for the underlying disc temperature to drop sufficiently to match the data. We note that including an albedo less than unity (which would be required for a spectrum as hard as $\ell_{\rm h}/\ell_{\rm s} = 7$) will only strengthen this conclusion, as the thermalized emission adds to the intrinsic seed photons to steepen the spectrum.

5.2 DISKEQ with coupled disc–corona over the inner disc

This tension between the observed spectral peak and observed luminosity is illustrated when we try to fit the spectrum with a disc–corona which extends down to $R_{\rm in} = R_{\rm ISCO}$ (left-hand panel of Fig. 1). We fix the spin to $a_* = 0$, as required in the high/soft state data, and fix the reflection parameters to $\xi = 300$, with smearing of $R_{\rm in} = 10\,R_{\rm g}$ and $\beta = 3$ (all as used in previous papers including Yamada et al. 2009 and T12). We first assume fully non-thermal injection ($\ell_{\rm nth}/\ell_{\rm h} = 1$). This does not give a good fit, with $\chi^2/{\rm dof} = 456.4/201$ for the reasons outlined above. The steep tail fixes $\ell_{\rm h}/\ell_{\rm s} \sim 0.5$, so $g \sim 0.3$ and the seed photons for the Comptonization are only slightly cooler (factor 0.91) than for a full disc. Allowing $\ell_{\rm nth}/\ell_{\rm h}$ to additionally be free did not give a substantial improvement, with best fit consistent with pure non-thermal injection. Allowing the disc ionization to be free switches the fit to being reflection dominated, which does not then conserve energy since most of the continuum which produces the observed enhanced reflection is not included in the energy budget. Since none of these fits are acceptable, we do not give detailed parameters.

We can have an acceptable fit if we allow the spin to be a free parameter. The best fit is then $\chi^2 = 228.1/200$ for $a^* = -1$ (i.e. extreme retrograde rotation). The detailed parameters are shown in column (1) in Table 3. Maximally retrograde spin has $R_{\rm ISCO} = 9\,R_{\rm g}$, which is 1.5 times larger than the disc-dominated state, possibly indicating that the disc is somewhat truncated in the VHS or that the stress heating prescription has changed markedly in the inner disc. However, using spin as a proxy for this transition radius is somewhat restrictive as this only allows values $<9\,R_{\rm g}$. We allow the model normalization to additionally be free, and discuss in the appendix how to use this to estimate the radius at which the stresses stop heating the accretion flow. This fits only slightly better ($\chi^2/{\rm dof} = 224.8/200$), showing that the spectrum is consistent with a stress free truncation of the emissivity at $\sim 9\,R_{\rm g}$. The best-fitting parameters and the residuals between the data and model are shown in column (2) in Table 3 and Fig. 6(b), respectively.

5.3 DISKEQ with coupled disc–corona and hot inner flow extending down to the ISCO

The previous section shows that the data are compatible with a model where the stresses change dramatically in the VHS, so that the flow is heated with a stress-free boundary at $R \sim 9$–$10\,R_{\rm g}$ rather than the $6\,R_{\rm g}$ expected from the known spin calibration. However, this could also indicate instead that the stresses are as expected for the black hole spin, but that the accretion flow makes a transition from the coupled disc–corona to a hot inner flow at radii $>9\,R_{\rm g}$, as required for the QPO models. Also, this would require that this flow is strongly radiatively inefficient so as to compensate for the

Table 3. Same as Table 1 but for the *Suzaku* VHS spectrum with DISKEQ.

Component	Parameter	outer disc + disc–corona (1) free spin	outer disc + disc–corona (2) scale correction	outer disc + disc–corona + flow (3) untruncated	outer disc + disc–corona + flow (4) truncated
TBABS	$N_{\rm H}(10^{21}\ {\rm cm}^{-2})$	$6.85^{+0.14}_{-0.15}$	$6.93^{+0.22}_{-0.15}$	(6.8)	(6.8)
RFXCONV[a]	$\Omega/2\pi$	$1.59^{+0.19}_{-0.17}$	$1.61^{+0.18}_{-0.17}$	$0.61^{+0.16}_{-0.13}$	$0.68^{+0.09}_{-0.14}$
DISKEQ[b]	$l_{\rm h}/l_{\rm s}$	0.45 ± 0.02	$0.44^{+0.03}_{-0.05}$	$0.46^{+0.03}_{-0.10}$	$0.45^{+0.02}_{-0.05}$
	$\tau_{\rm cor}$	0.67 ± 0.04	$0.63^{+0.07}_{-0.13}$	$0.46^{+0.09}_{-0.23}$	$0.46^{+0.05}_{-0.10}$
	$\tau_{\rm in}$	–	–	$2.78^{+0.11}_{-0.25}$	$2.66^{+0.07}_{-0.43}$
	$f_{\rm rad}$	–	–	0.26 ± 0.03	(1)
	$R_{\rm cor}(R_{\rm g})$	48^{+4}_{-5}	$50^{+7}_{-4} \times$ scale	49^{+8}_{-5}	$46^{+7}_{-4} \times$ scale
	$R_{\rm flow}(R_g)$	–	–	$24.5^{+1.8}_{-2.4}$	$18.5^{+1.8}_{-0.7} \times$ scale
	$\dot{M}(10^{18}\ {\rm gs}^{-1})$	$6.48^{+0.11}_{-0.13}$	$6.0^{+0.7}_{-1.1} \times$ scale	$5.97^{+0.16}_{-0.25}$	$6.3^{+0.6}_{-0.7} \times$ scale
	a^*	$-1^{+0.15}_{-0({\rm hardlimit})}$	(-1)	(0)	(-1)
	Scale	(1)	$1.05^{+0.11}_{-0.07}$	(1)	$1.01^{+0.07}_{-0.05}$
	Estimated $R_{\rm in}(R_g)$[c]	$9^{+0({\rm hardlimit})}_{-0.43}$	$9.5^{+0.9}_{-0.7}$	(6)	$9.0^{+0.7}_{-0.4}$
Absorbed 0.7–100 keV flux	$10^{-8}\ {\rm erg\,s^{-1}\,cm^{-2}}$	2.62	2.63	2.61	2.61
Unabsorbed 0.7–100 keV flux	$10^{-8}\ {\rm erg\,s^{-1}\,cm^{-2}}$	3.56	3.59	3.54	3.55
Unabsorbed 0.1–200 keV flux	$10^{-8}\ {\rm erg\,s^{-1}\,cm^{-2}}$	4.56	4.61	4.52	4.54
χ^2/dof		228.1/200	224.8/200	184.0/199	183.6/199

Note. Values in parenthesis are fixed. Energy is extended from 0.1 to 1000 keV. Distance and inclination are assumed to be $D = 8$ kpc and $i = 50^\circ$. [a]Smeared reflection is same as Table 1, but ionization parameter is fixed at $\xi = 300$. KDBLUR is used with $R_{\rm in} = 10\,R_{\rm g}$ and $R_{\rm in} = R_{\rm flow}$ for with and without inner flow, respectively. [b]Values of normalization factor, $\ell_{\rm nth}/\ell_{\rm h}$, and $\Gamma_{\rm inj}$, are fixed to be 1287, 1, and 3.5, respectively. [c]The value of $R_{\rm in}$ is estimated by the ISCO for the given spin parameter a^* as $R_{\rm ISCO} \times$ scale.

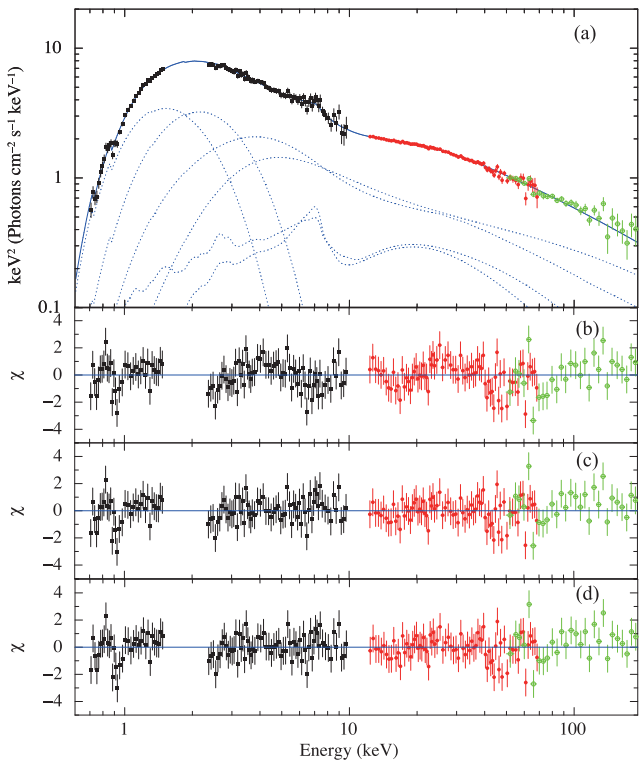

Figure 6. νF_ν spectrum of GX 339 − 4 in the VHS based in the best-fitting DISKEQ with stress-free truncated flow (panel a). Residuals between data and the best-fitting DISKEQ model without inner flow, with inefficient inner flow, and with stress-free truncated flow are shown in panels (b), (c), and (d), respectively. In panel (a), PIN (red filled circle) and GSO (green open circle) data are normalized to XIS data (black filled square).

additional energy released between a stress-free truncation at $6\,R_{\rm g}$ as expected from Novikov–Thorne, and the stress-free truncation at $\sim 9\,R_{\rm g}$ which fits the data above.

We fix $a^* = 0$, and $\ell_{\rm nth}/\ell_{\rm h} = 1$ but now allow the disc–corona region to be truncated, with additional inverse Compton emission from the innermost region between the disc truncation radius and the ISCO (see the schematic geometry in Fig. 1b). We assume that the inner region also has completely non-thermal electron acceleration, with $\ell_{\rm nth}/\ell_{\rm h} = 1$, again with fixed reflection ionization and smearing (now tied to the inner edge of the disc–corona, i.e. $R_{\rm flow}$). There are then two remaining parameters which control the shape of the spectrum from the inner flow, namely $\tau_{\rm in}$ and $(\ell_{\rm h}/\ell_{\rm s})_{\rm in}$. These cannot be constrained independently so we choose to tie $(\ell_{\rm h}/\ell_{\rm s})_{\rm in}$ to $\ell_{\rm h}/\ell_{\rm s}$ in the disc–corona region and let $\tau_{\rm in}$ be free. In addition, we fixed absorption column at $N_{\rm H} = 6.8 \times 10^{21}\ {\rm cm}^{-2}$, the average value seen in the high/soft state. Thus the free parameters increase only by 1.

This gives an excellent fit to the data (column 3 in Table 3), with χ^2/dof = 184.0/199, with reasonable reflection ($\Omega/2\pi = 0.61$). The coupled disc–corona region extends from 49–25 $R_{\rm g}$, with a radiatively inefficient ($f_{\rm rad} = 0.26$) hot flow from 25–6 $R_{\rm g}$. The optical depth of the inner corona is estimated at $\tau_{\rm in} = 2.8$, significantly larger than for the disc–corona, where $\tau_{\rm cor} = 0.43$, though we caution that this simply means that the inner flow has a spectrum which is slightly different to that of the disc–corona.

The best-fitting value of $\ell_{\rm h}/\ell_{\rm s} = 0.46$ gives $g = 0.32$. Together with the best fit $\tau = 0.46$ this gives an estimate for the intrinsic fraction of power dissipated in the corona of $f \sim 0.3$–0.4 for an albedo of 1–0 (see Appendix B).

5.4 DISKEQ with coupled disc–corona and efficient hot inner flow truncated at the bending wave radius

Detailed fits to the variability power spectrum of a VHS of similar QPO frequency in XTE J1550−564 gives $\sim 13\,R_{\rm g}$ for the transition

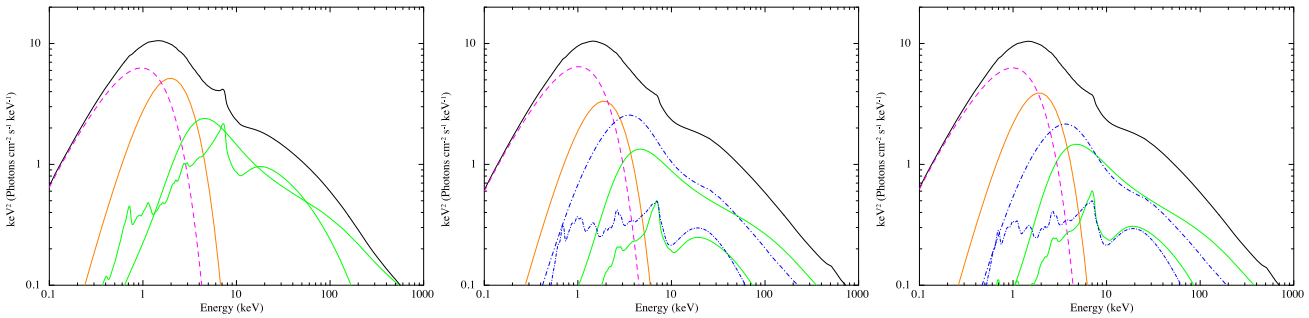

Figure 7. Unabsorbed spectral models for the *Suzaku* VHS spectrum based on best-fitting model of DISKEQ without inner flow (left), with inefficient untruncated inner flow (middle), and with stress-free truncated inner flow (right). Model components are the outer disc (dashed magenta), inner disc underneath the coupled disc–corona region (solid orange), coupled hybrid corona and its reflection (solid green), inner flow and its reflection (dash–dotted blue lines).

between the disc and inner flow (Obs 5 in Ingram & Done 2012). However, these QPO models also rely on the misaligned flow not extending down to the ISCO but being truncated at the bending wave radius, where the torques become so strong as to truncate the flow. This is $\sim 12\,R_{\rm g}$ in the matching observation of XTE J1550−564, so the inner flow in their picture is a narrow ring from 13 to $12\,R_{\rm g}$ (Ingram & Done 2012). This picture is somewhat different to that modelled above, where the hot flow which extends down to the ISCO but can be radiatively inefficient.

It is not at all clear what should happen to the accretion torques in the inner part of a misaligned flow below the bending wave radius. There are additional stresses at the bending wave radius, and then below this the flow free streams into the black hole (Fragile et al. 2007; Dexter & Fragile 2011). Thus it seems possible that the stresses might be more like a stress-free inner boundary at the bending wave radius, or it may be that the additional stresses at the bending wave radius release all the remaining energy (Fragile, private communication). The model above assumes the latter, that all the accretion energy is released in the hot flow, in which case most of this energy is not radiated as hard X-rays. Instead, we now explore the possibility that the flow truncation at the bending wave radius changes the dissipation to something more like a stress-free inner boundary condition at the bending wave radius (see Fig. 1c).

We again use the spin parameter to model the effect of a stress free inner boundary condition at $R > R_{\rm ISCO}$. We again find a good solution ($\chi^2/{\rm dof} = 183.6/199$) with $a^* = -1$, i.e. implying stress-free emissivity with truncation radius of $9\,R_{\rm g}$ where the inner region is now radiatively efficient (as there is much less energy), with $f_{\rm rad} = 1$. The νF_ν spectrum deconvolved with this model is shown in Fig. 6 (panel a), while the residuals are shown in panel (d). The unabsorbed model components are shown in the right-hand panel of Fig. 7, and best-fitting parameters are listed in column (4) in Table 3. These show the coupled disc–corona region extends from 19 to $46\,R_{\rm g}$, while the innermost flow extends from ∼9 to $19\,R_{\rm g}$.

5.5 The importance of reflection modelling

The results shown in Sections 5.3 and 5.4 indicate that the efficiency of the accretion disc decreases below the expected Novikov-Thorne efficiency. One of the scenarios to explain this inefficient inner flow is that a fraction of the accretion power is used instead to power the jet. The energy loss inferred from the central flow is of order the radiated luminosity. Thus we need to determine the coronal power to better than a factor of 2 to constrain this energy loss. However, reflection can contribute to the hard X-rays with luminosity of the same order as the accretion power, so treating reflection correctly is important.

We can get an upper limit to the coronal power by removing reflection, and just using an apparent SMEDGE and Gaussian to get the spectrum to fit. We checked our results on the coupled disc–corona model with inefficient/efficient hot inner flow (Sections 5.3 and 5.4). In the case of the inefficient untruncated inner flow (see Section 5.3 and column 3 in Table 3), the radiative efficiency of the inner flow is found to be larger, but still significantly below unity, with $f_{\rm rad} = 0.42^{+0.01}_{-0.06}$ with $\ell_{\rm h}/\ell_{\rm s} = 0.71^{+0.10}_{-0.08}$ ($g = 0.42 \pm 0.03$) under the similar disc–corona geometry with $R_{\rm cor} = 42 \pm 4\,R_{\rm g}$ and $R_{\rm flow} = 28^{+6}_{-5}\,R_{\rm g}$. Similarly, in the case of the efficient truncated inner flow (Section 5.4, column 4 in Table 3), the inner radius of the efficient hot inner flow is estimated to be $R_{\rm in} = 8.6^{+0.6}_{-0.5}\,R_{\rm g}$ with $\ell_{\rm h}/\ell_{\rm s} = 0.69^{+0.12}_{-0.08}$ ($g = 0.41^{+0.04}_{-0.03}$). The larger radiated power required by removing reflection means that $R_{\rm in}$ becomes smaller, but it is still strongly required to be truncated. Thus even allowing no contribution from reflection, the radiated power inferred is still significantly less than that required by the NT emissivity.

Conversely, the maximum reflection will give the minimum radiated power, and hence the maximum decrease in efficiency from NT. We neglected reflection from the overlap coupled disc–corona region which is acceptable only if the reflector has such high ionization parameter that it is completely reflective (as assumed) or that the optical depth of the corona is large. Given that the optical depth of our corona is not large, at $\tau \sim 0.46$ (see columns 3 and 4 in Table 3), we explore whether we can increase the contribution of reflection by incorporating reflection from the coupled disc–corona region. Hence we refit the data based on the model described in Sections 5.3 and 5.4 by changing the inner radius of the smeared reflection from $R_{\rm flow}$ to $R_{\rm cor}$. Slightly worse fits are obtained as $\chi^2/{\rm dof} = 188.1/199$ and $189.2/199$ for the inefficient and efficient inner flow, respectively. However, the values of the efficiency and the truncated radius are obtained as $f_{\rm rad} = 0.27 \pm 0.03$ and $R_{\rm in} = 8.9^{+0.7}_{-0.2}\,R_{\rm g}$, respectively, the values which are the same as previous fits within 90 per cent uncertainties (see columns 3 and 4 in Table 3).

6 DISCUSSION

6.1 Summary of the results

Fitting physical models for the complex spectra seen in the VHS offers new insight into the properties of this complex state. Our model offers two main improvements on earlier attempts: first, it models the Comptonized emission with the EQPAIR code, which self-consistently calculates the electron distribution from non-thermal acceleration. This is not a power law, as assumed in SIMPL Comptonization, but is hybrid as the low-energy electrons thermalize by

Coulomb rather than Compton cooling. This has a profound impact on the derived reflection parameters. Rather than requiring that the source be reflection dominated, and that the reflection is strongly smeared, the EQPAIR models (which fit the data better than the SIMPL models) have $\Omega/2\pi = 0.8$ and only moderate smearing which does not constrain black hole spin. We caution that spin determinations from reflection parameters are not always robust to changes in the continuum model.

The second improvement in our code is that it specifically sets the available energy in terms of the physical black hole parameters, assuming a Novikov–Thorne emissivity. This is clearly appropriate for the high/soft state taken a few days after our VHS observation. A comparison of these two spectra using the same physical black hole parameters is especially compelling as they have similar luminosities. The high/soft state is disc dominated, so the emissivity is dissipated as (colour temperature corrected) blackbody emission at each radius. A blackbody is the most efficient radiator so a spectrum with the same luminosity cannot have a mean photon energy which is lower than this. Since the VHS spectrum is steep, this means that the similar luminosity VHS spectrum cannot peak at a lower energy if the dissipation as a function of radius remains unaltered. The observed drop in energy at which the VHS spectrum peaks compared that of the thermal high/soft state at a similar luminosity then clearly shows that the energy dissipated in the accretion flow as a function of radius has changed dramatically from that of Novikov–Thorne. Simply growing a corona, even one whose energy and seed photons are coupled to the underlying disc emission, will produce a spectrum which peaks at higher energy than that of the multiblackbody disc seen in the high/soft state. Even making a transition from the coupled disc–corona to a hot inner flow still cannot fit the data unless the dissipation changes, fundamentally because a blackbody is the most efficient radiator, so any other radiation mechanism will only increase the peak spectral energy for the same luminosity.

There are three possible ways to match what is observed. First, the total dissipation could still be Novikov–Thorne if most of the power released in the innermost radii does not go to heating the accretion flow but is instead 'dark', e.g. lost as kinetic energy in a jet/wind. Secondly, the dissipation could be changed from Novikov–Thorne in the inner regions e.g. if the flow is misaligned and truncation at the bending wave radius sets an effective stress-free inner boundary to the flow at $R > R_{\rm ISCO}$. Both these require that the radiated efficiency has dropped compared to Novikov–Thorne, so the same luminosity as the high/soft state can only be produced with a higher mass accretion rate through the outer (standard) disc. The third possibility is that the flow is not in steady state, so that the mass accretion rate in outer disc is larger than that in the inner disc. We discuss each of these in turn below.

6.2 Low radiative efficiency: jet power?

The most obvious solution to the observed discrepancy in luminosity between the inner and outer flow is that the additional power is lost up the jet. The kinetic power of the jet is poorly constrained, but may be of order the accretion power (Fender et al. 2004). This would imply that the jet is accretion powered, rather than tapping the spin energy of the black hole (Blandford–Znajek).

The source here is still showing type C QPOs, so has not made an HIMS/SIMS transition which is (loosely) associated with the collapse of the radio jet, so on timing signatures alone the source could still be powering a steady, compact jet. However, there are simultaneous radio observations which show that the jet is already strongly suppressed by this point (Corbel: private communication). The 3–9 keV observed X-ray flux of 7.9×10^{-9} ergs s^{-1} cm^{-2} predicts a 9 GHz radio flux of 15 mJy from the Fundamental Plane (Corbel et al. 2013a). Removing the disc component so as to include only the Comptonized power still gives a 3–9 keV flux of 7.4×10^{-9} erg s^{-1} cm^{-2}, so this does not make a significant difference to the predicted radio flux. Yet the observed 9 GHz flux on February 15 (simultaneous with the end of the *Suzaku* observation) is 1.4 mJy (Corbel, private communication), so it appears that the radio is already strongly suppressed below the Fundamental Plane at this point. Thus our missing luminosity is not powering the steady, compact jet. We note that a similar drop in radio without being accompanied by any change in X-ray variability power and QPO type is also seen in MAXI J1659 − 152(van der Horst et al. 2013).

Instead, the timing transition may be associated with the launching of the discrete ejection events (Fender, Homan & Belloni 2009; Miller-Jones et al. 2012), which gives another potential energy/mass-loss process. However, our VHS observation is still in the HIMS, with strong X-ray variability and type C QPO. The transition to the SIMS happens up to a day after our VHS observation (Motta et al. 2011), and indeed, the radio data just before and just after the high/soft state on February 19 show an optically thin radio flare (16 and 12 mJy at 9 GHz on February 18 and 20). Thus if the HIMS/SIMS transition marks the ejection, our data are not losing energy via this route as the transition has not yet taken place.

However, we note that radio behaviour around the transition is complex, and that there are time lags between various components of the jet which can make it difficult to establish causal connections (Hannikainen et al. 2009; Miller-Jones et al. 2012; Brocksopp et al. 2013; Corbel et al. 2013b; Curran et al. 2015). None the less, it seems that the power is not being dissipated in a steady jet, nor in a discrete ejection. Our *Suzaku* data are taken over a time-scale of 3 d without much change in spectral or timing properties (Motta et al. 2011; T12), so it seems unlikely that there was a missed transition and then recovery back to the HIMS.

There do not appear to be any other obvious energy loss channels. The inferred mass accretion rate (modulo the uncertainties in system parameters) does not seem to be at or above Eddington, so optically thick advection (Abramowicz et al. 1988), or mass-loss through radiatively driven winds (Shakura & Sunyaev 1973) are not likely to make much of a difference to the radiated power, though magnetic winds from the inner disc are always a possibility. Conversely, the system luminosity is high enough that substantial losses through optically thin advection are not likely either (Narayan & Yi 1995; Yuan & Zdziarski 2004). Thus a magnetically driven outflow/jet appears to be the only candidate, and this needs to carry away around as much energy as is radiated.

6.3 A stress-free inner boundary at $R > R_{\rm ISCO}$

The Novikov–Thorne emissivity is specifically derived for a thin disc, where the stresses which give rise to viscosity are in a plane. A geometrically thick flow can have very different stresses e.g. a large-scale height flow can have magnetic connections across the horizon, so the stress-free inner boundary condition is no longer appropriate (Krolik, Hawley & Hirose 2005; Shafee et al. 2008). However, this leads to additional dissipation, rather than to less dissipation, as required here.

Our preferred flow model is complex, with a thin disc, transitioning to a coupled disc–corona region. The thin disc then disappears completely in the inner region, leaving only corona plasma between $R_{\rm flow}$ and $R > R_{\rm ISCO}$. It is not at all clear what happens to the

dissipation at the edge of the thin disc $R_{\rm flow}$. The hotter plasma may support stresses like the Novikov–Thorne stresses across the boundary between them, or it may be rarified enough that a stress-free inner boundary condition at the truncation radius is more appropriate. In the latter case, the accretion power on the inner edge of the disc–corona and the outer part of the hot flow is lower than expected from Novikov–Thorne, though this might not be a large enough effect to produce the required marked deficit in power.

Instead, the mismatch between mass accretion rate and luminosity in the inner flow could be produced in the three zone models as an additional signature of a Lense–Thirring origin of the QPO. A flow which is misaligned to the black hole spin experiences a torque, which propagates at the local sound speed. A thin disc is cool, so the bending waves cannot propagate fast enough to make the disc precess, so it forms a stable warp (Bardeen–Petterson). Conversely, for a thick disc, the hotter material means a faster sound speed, so the torque can communicate across the flow on time-scales fast enough for it to precess as a solid body (Fragile et al. 2007; Ingram et al. 2009). The misalignment torques are so strong at small radii that they effectively truncate the flow at a bending wave radius, of the order of 8–12 $R_{\rm g}$ (Fragile et al. 2007, 2009; Ingram et al. 2009; Dexter & Fragile 2011; Ingram & Done 2012). The accretion flow is laminar rather than turbulent after this point, so it may lead to an effective stress-free inner boundary condition at a radius larger than $R_{\rm ISCO}$, giving less accretion power. However, the torques could also simply transfer the accretion power from below to above the bending wave radius, so that the total dissipation in the flow remained similar to that expected from Novikov–Thorne (Fragile, private communication).

6.4 Applicability of Novikov–Thorne emissivity

The two possibilities discussed above both require that the overall efficiency is lower than Novikov–Thorne. Fundamentally this conclusion is driven by the observation that the VHS spectrum peaks at lower energy than that seen in the similar luminosity high/soft state. The observed continuum below 1 keV is sensitive to the mass accretion rate through the outer (standard disc). The Novikov–Thorne emissivity should be appropriate here, yet fits constrain the mass accretion rate through the outer disc to be $\sim$1.5 $\times$ higher than that required to power the high/soft state (see Tables 1 and 3). Since the observed luminosity of the VHS is only $\sim$1.1 $\times$ that of the high/soft state, then this requires that the radiative efficiency is lower in the inner disc.

However, a decreasing mass accretion rate from the VHS to the high/soft state while the bolometric luminosity stays almost the same appears somewhat fine tuned. Instead, since our data are taken on the fast rise to outburst, the flow could simply be out of steady state, while Novikov–Thorne explicitly assumes constant $\dot{M}$ at all radii. Simulations of the viscous evolution of the disc during an outburst show that the surface density takes days to settle into this configuration after the hydrogen ionization instability is triggered at large radii (Dubus, Hameury & Lasota 2001). None the less, our VHS data are taken over a 3 d time period with little evolution in spectra or timing properties, so it seems more likely that the flow is in some sort of steady state.

6.5 Distinguishing between these possibilities

The VHS is a rather rare spectral state. More observations would clearly show whether the difference in emissivity seen here is only associated with fast changes in mass accretion rate, as is required in Section 6.4. Similarly, more simultaneous radio observations would tie down the associated jet and/or plasma ejections required in Section 6.2, though the magnetic wind is much harder to constrain. A stress-free inner boundary due to bending wave radius from a misaligned precessing hot flow (Section 6.3) should also be present in any QPO observation of the low/hard state.

7 CONCLUSIONS

Comptonization in the VHS is complex, with a high-energy tail pointing to the importance of non-thermal electrons. However, purely non-thermal acceleration does not result in a purely power-law electron distribution when both Compton and Coulomb collisions are included. The self-consistent (pure power-law acceleration balancing cooling) steady-state electron distribution is thermal at low energies, resulting in a Compton continuum with complex curvature, as calculated in the EQPAIR code by Coppi. This completely removes the requirement for high black hole spin and high reflected fraction in the *Suzaku* VHS data.

We develop a new model for the accretion flow, DISKEQ which tracks energy across the flow but allows this to be dissipated either in a standard disc, or in a coupled disc–corona geometry where the Comptonization is based on the EQPAIR code or in a hot inner flow, where again the Comptonization is described by EQPAIR. Using this, we demonstrate for the first time that the VHS is not well described by Novikov–Thorne emissivity. The spectrum below 1 keV constrains the outer (standard) disc emission, requiring a mass accretion rate which is 1.5 $\times$ higher than that seen in a disc-dominated high/soft state, but the total VHS spectrum is only a factor 1.1 $\times$ brighter. The most obvious solution is that the excess Novikov–Thorne emissivity in the inner disc is not translated into radiation, but is instead used to power of the jet. However, simultaneous observations show that the radio is strongly suppressed. Instead, it could show that the Novikov–Thorne prescription is not appropriate, perhaps due to the flow being misaligned as required to produce the QPO from Lense–Thirring precession.

We urge the use of more physical models to fit the complex intermediate states in order to distinguish between these possibilities, and are releasing the code within the XSPEC spectral fitting package to enable this.

ACKNOWLEDGEMENTS

We are grateful to Julien Malzac as a referee for his valuable and helpful comments and suggestions, especially for the derivation in Appendix B. We thank Mari Kolehmainen for giving us the high/soft state spectrum of GX 339 − 4, and Stephane Corbel for giving us a radio data. We also thank Shin'ya Yamada for his helpful advice on GSO analyses, and Chris Fragile for insight into the simulations. AK and CD acknowledge support from Grant-in-Aid No. 24540237 from Ministry of Education, Culture, Sports, Science and Technology of Japan. CD also acknowledges support from the STFC consolidated grant ST/L00075X/1.

REFERENCES

Abramowicz M. A., Czerny B., Lasota J. P., Szuszkiewicz E., 1988, ApJ, 332, 646
Brenneman L. W., Reynolds C. S., 2006, ApJ, 652, 1028
Brocksopp C., Corbel S., Tzioumis A., Broderick J. W., Rodriguez J., Yang J., Fender R. P., Paragi Z., 2013, MNRAS, 432, 931
Coppi P. S., 1992, MNRAS, 258, 657
Corbel S., Coriat M., Brocksopp C., Tzioumis A. K., Fender R. P., Tomsick J. A., Buxton M. M., Bailyn C. D., 2013a, MNRAS, 428, 2500
Corbel S. et al., 2013b, MNRAS, 431, L107

Curran P. A. et al., 2015, MNRAS, 451, 3975
Dexter J., Fragile P. C., 2011, ApJ, 730, 36
Done C., Kubota A., 2006, MNRAS, 371, 1216
Done C., Gierliński M., Kubota A., 2007, A&AR, 15, 1
Done C., Davis S. W., Jin C., Blaes O., Ward M., 2012, MNRAS, 420, 1848
Done C., Jin C., Middleton M., Ward M., 2013, MNRAS, 434, 1955
Dubus G., Hameury J.-M., Lasota J.-P., 2001, A&A, 373, 251
Esin A. A., McClintock J. E., Narayan R., 1997, ApJ, 489, 865
Fender R. P., Belloni T. M., Gallo E., 2004, MNRAS, 355, 1105
Fender R. P., Homan J., Belloni T. M., 2009, MNRAS, 396, 1370
Fragile P. C., Blaes O. M., Anninos P., Salmonson J. D., 2007, ApJ, 668, 417
Fragile P. C., Lindner C. C., Anninos P., Salmonson J. D., 2009, ApJ, 691, 482
Gallo E., Fender R. P., Pooley G. G., 2003, MNRAS, 344, 60
Gardner E., Done C., 2013, MNRAS, 434, 3454
Gierliński M., Done C., 2003, MNRAS, 342, 1083
Haardt F., Maraschi L., 1993, ApJ, 413, 507
Hannikainen D. C. et al., 2009, MNRAS, 397, 569
Hjalmarsdotter L., Axelsson M., Done C., 2016, MNRAS, 456, 4354
Ingram A., Done C., 2012, MNRAS, 419, 2369
Ingram A., Done C., Fragile P. C., 2009, MNRAS, 397, L101
Kokubun M. et al., 2007, PASJ, 59, 53
Kolehmainen M., Done C., 2010, MNRAS, 406, 2206
Kolehmainen M., Done C., Díaz Trigo M., 2011, MNRAS, 416, 311
Krolik J. H., Hawley J. F., Hirose S., 2005, ApJ, 622, 1008
Kubota A., Done C., 2004, MNRAS, 353, 980
Kubota A., Makishima K., 2004, ApJ, 601, 428
Kubota A., Tanaka Y., Makishima K., Ueda Y., Dotani T., Inoue H., Yamaoka K., 1998, PASJ, 50, 667
Kubota A., Makishima K., Ebisawa K., 2001, ApJ, 560, L147
Laor A., 1991, ApJ, 376, 90
Li L.-X., Zimmerman E. R., Narayan R., McClintock J. E., 2005, ApJS, 157, 335
Ludlam R. M., Miller J. M., Cackett E. M., 2015, ApJ, 806, 262
Miller-Jones J. C. A. et al., 2012, MNRAS, 421, 468
Mitsuda K. et al., 1984, PASJ, 36, 741
Motta S., Muñoz-Darias T., Casella P., Belloni T., Homan J., 2011, MNRAS, 418, 2292
Narayan R., Yi I., 1995, ApJ, 452, 710
Novikov I. D., Thorne K. S., 1973, in Dewitt C., Dewitt B. S., eds, Black Holes (Les Astres Occlus), Astrophysics of black holes. Gordon and Breach, New York, p. 343
Poutanen J., Svensson R., 1996, ApJ, 470, 249
Remillard R. A., McClintock J. E., 2006, ARA&A, 44, 49
Shafee R., McKinney J. C., Narayan R., Tchekhovskoy A., Gammie C. F., McClintock J. E., 2008, ApJ, 687, L25
Shakura N. I., Sunyaev R. A., 1973, A&A, 24, 337
Shimura T., Takahara F., 1995, ApJ, 445, 780
Steiner J. F., Narayan R., McClintock J. E., Ebisawa K., 2009, PASP, 121, 1279
Svensson R., Zdziarski A. A., 1994, ApJ, 436, 599
Tamura M., Kubota A., Yamada S., Done C., Kolehmainen M., Ueda Y., Torii S., 2012, ApJ, 753, 65 (T12)
van der Horst A. J. et al., 2013, MNRAS, 436, 2625
Wilms J., Allen A., McCray R., 2000, ApJ, 542, 914
Yamada S. et al., 2009, ApJ, 707, L109
Yamada S. et al., 2011, PASJ, 63, 645
Yuan F., Zdziarski A. A., 2004, MNRAS, 354, 953
Zdziarski A. A., Grove J. E., Poutanen J., Rao A. R., Vadawale S. V., 2001, ApJ, 554, L45

APPENDIX A: APPROXIMATION OF THE TRUNCATED RADIUS WITH FRICTION FREE INNER BOUNDARY CONDITION

We allow the distance d to be an additional free parameter in order for it to act as a proxy for the truncation radius of a flow/disc with stress free inner boundary at $R > R_{\rm ISCO}$, for the fixed spin parameter $a^* = -1$. The scaling factor in Table 3 is defined as $(d/8\ {\rm kpc})^{-1}$, and the proper radii are approximately estimated by multiplying the scaling factor to the derived radii with DISKEQ.

APPENDIX B: THE IMPACT OF REPROCESSING/REFLECTION ON $\ell_{\rm h}/\ell_{\rm s}$ IN THE COUPLED DISC–CORONA

The ratio $\ell_{\rm s}/\ell_{\rm h}$ is the major parameter determines the spectral shape from Comptonization. In the overlap region, reflection and reprocessing mean that this is not simply related to the fraction f of the intrinsic power which is dissipated in the corona. At the disc surface, the outgoing flux $\ell_{\rm disc}^{\rm out}$ is the sum of the intrinsic disc dissipation, $\ell_{\rm si}$, and the reflected/reprocessed response of the disc to the irradiating flux from the corona, $\ell_{\rm rep}$, and reflected component, $\ell_{\rm R}$. Hence $\ell_{\rm disc}^{\rm out} = \ell_{\rm si} + \ell_{\rm R} + \ell_{\rm rep} = \ell_{\rm s} + \ell_{\rm R}$ as the total soft flux is the sum of the seed and reprocessed emission. By using disc irradiation from the corona, $\ell_{\rm ir}$, $\ell_{\rm R}$ can be written as $\ell_{\rm R} = a\ell_{\rm ir}$ for an albedo a, and $\ell_{\rm ir}$ is the sum of downwards flux from intrinsic dissipation, plus the energy of the seed photons backscattered from the disc. Hence, considering the fraction of disc and reflection luminosity scattered in the corona, $\ell_{\rm scat} = (\ell_{\rm s} + \ell_{\rm R})(1 - e^{-\tau})$, the irradiation from the corona is written as following.

$$\ell_{\rm ir} = \ell_{\rm h}/2 + (1 - e^{-\tau})\ell_{\rm disc}^{\rm out}/2 = \ell_{\rm h}/2 + (1 - e^{-\tau})(\ell_{\rm s} + a\ell_{\rm ir})/2$$

Recasting this as an explicit equation gives

$$\frac{\ell_{\rm ir}}{\ell_{\rm h}} = \frac{1 + (\ell_{\rm s}/\ell_{\rm h})(1 - e^{-\tau})}{2 - a + ae^{-\tau}} = \frac{e^{-\tau} + (1 - e^{-\tau})/g}{2 - a + ae^{-\tau}}$$

defining $g = \ell_{\rm h}/(\ell_{\rm h} + \ell_{\rm s})$, similar to the equation $f = \ell_{\rm h}/(\ell_{\rm h} + \ell_{\rm si})$ for the intrinsic dissipation. Since $\ell_{\rm si} = \ell_{\rm s} - \ell_{\rm rep}$ then $f = g(1 - g(1 - a)\ell_{\rm ir}/\ell_{\rm h})^{-1}$. Substituting from above for $\ell_{\rm ir}/\ell_{\rm h}$ gives

$$f = g\frac{2 - a + ae^{-\tau}}{1 + e^{-\tau} - g(1 - a)e^{-\tau}}$$

(J. Malzac, private communication).

The power emitted from the top of the corona, $\ell_{\rm out}$, is now the sum of the coronal power plus the seed photons travelling upwards, $(\ell_{\rm h} + \ell_{\rm scatt})/2$, together with the disc emission crossing the corona without any interaction, $(\ell_{\rm s} + \ell_{\rm R})e^{-\tau}$. The total disc emission is caused by internal dissipation and irradiation so $\ell_{\rm s} + \ell_{\rm R} = \ell_{\rm si} + \ell_{\rm ir}$. Substituting for $\ell_{\rm ir}$ from above gives $\ell_{\rm s} + \ell_{\rm R} = 2(\ell_{\rm si} + \ell_{\rm h}/2)/(1 + e^{-\tau})$ so that $\ell_{\rm out} = \ell_{\rm si} + \ell_{\rm h}$. Hence energy is still conserved in this region, as assumed in the code (J. Malzac, private communication). However, our code does not explicitly distinguish the internally reflected emission, $\ell_{\rm R}$, from $\ell_{\rm h}$, and we caution that full radiative transfer is probably required in this region.

This paper has been typeset from a TEX/LATEX file prepared by the author.